




RESEARCH ARTICLE

WILEY

The Global Atlas for Siting Parameters project: Extreme wind, turbulence, and turbine classes

Xiaoli Guo Larsén¹  | Neil Davis¹ | Ásta Hannesdóttir¹  | Mark Kelly¹  |
Lasse Svenningsen² | René Slot² | Marc Imberger¹ | Bjarke Tobias Olsen¹ |
Rogier Floors¹

¹Wind Energy Department, Technical University of Denmark, Risø Campus, Roskilde, Denmark

²EMD International A/S, Aalborg, Denmark

Correspondence

Xiaoli Guo Larsén, Frederiksborgvej 399, Building 125, 4000 Roskilde, Denmark.
Email: xgal@dtu.dk

Funding information

Supported by Danish EUDP J. nr. 64018-0095

Summary

The Global Atlas for Siting Parameters project compiles a suite of models into a complex modeling system, uses up-to-date global datasets, and creates global atlases of siting parameters at a spatial resolution of 275 m. These parameters include the 50-year wind, turbulence, and turbine class recommendations based on relevant generic turbines. The suite of models includes the microscale Linear Computational Model (LINCOM), a statistical, spectral correction method here revised for strong convective areas and tropical cyclone affected areas, two turbulence models with four setups, and load models. To this complexity, an uncertainty model was developed to classify the various sources of uncertainties for both the extreme wind and the turbulence calculations, and accordingly, atlases of uncertainty classification were created. Preliminary validation of the global calculations of the 50-year wind and turbulence is done through comparisons with measurements, and the results are promising. This is the first time the siting parameters are obtained with such a high spatial resolution and shared on open data portal. It is expected to benefit the global wind energy planning and development.

KEYWORDS

extreme wind, global atlas, turbine class recommendation, turbulence

1 | INTRODUCTION

The GASP (Global Atlas of Siting Parameters) project aims at bringing down the Levelized Cost of Energy by providing data for turbine siting parameters. Siting parameters are needed to avoid placing turbines in a dangerous wind environment and to identify the suitable turbine design class, which is critical for evaluating the financial feasibility of a wind farm project. The design class is reflected not only on the purchase price and maintenance schedule for the turbines but also on the annual energy production that is related to the rotor diameters and hub heights. The National Renewable Energy Lab (NREL) reports the correct type of turbine can produce 50–60% more power than over-designed turbines with smaller diameters.¹ The GASP project helps to lower the risk of this over-design by reducing the critical mismatch between the turbine and the site. The global coverage and open access of data will benefit the overall wind energy development globally and in particular help countries and regions where wind energy has great potential but is still under-developed.

This is an open access article under the terms of the [Creative Commons Attribution](https://creativecommons.org/licenses/by/4.0/) License, which permits use, distribution and reproduction in any medium, provided the original work is properly cited.

© 2022 The Authors. *Wind Energy* published by John Wiley & Sons Ltd.

TABLE 1 Wind turbine design classes in IEC 61400-1 ed 4

Wind turbine class	I	II	III	S
V_{ave} (m s ⁻¹)	10.0	8.5	7.5	
V_{ref} (m s ⁻¹)	50.0	42.5	37.5	
$V_{ref,T}$ (m s ⁻¹) (Tropical)	57.0	57.0	57.0	Values specified by the designer
A+ I_{ref}		0.18		
A I_{ref}		0.16		
B I_{ref}		0.14		
C I_{ref}		0.12		

Note: The parameter values apply at hub height, and V_{ave} is the annual average wind speed; V_{ref} is the reference wind speed average over 10 min; $V_{ref,T}$ is the reference wind speed average over 10 min applicable for areas subject to tropical cyclones. A+ designates the category for very high turbulence characteristics; A for higher turbulence characteristics; B for medium turbulence characteristics; C for lower turbulence characteristics and I_{ref} is a reference value of the turbulence intensity.

Modern wind turbines are typically designed according to the requirements for class certification defined by the IEC 61400-1 design standard² as outlined in Table 1. There are three main classes of turbines based on the 50-year wind at a temporal resolution of 10 min at the hub height, each of which has sub-classes based on turbulence. Extreme winds and turbulence statistics are needed to determine what types of turbines will be able to withstand the site-specific wind loads.

Currently, site assessment of the normal and extreme wind climate relies heavily on the on-site measurements. This has several challenges, as measurement campaigns often focus on normal wind climate. Such measurements are often short-term, and they are not sensitive to some missing data during a few strong wind events when the measurement techniques can often be challenged. However, both long-term measurements and data during strong wind events are essential for assessing the extreme wind statistics, and they are rarely available. Moreover, most standard measurements do not either focus on turbulence.

The calculation of extreme wind data also suffers from inconsistent techniques and methods used by different countries, causing discontinuity in values at national borders, as Eurocode³ shows such a situation for European countries. To solve this problem, people have used long-term pressure measurements, as they are more often available than wind, to calculate the geostrophic wind and hereafter the standard winds (namely winds at 10 m over a homogeneous surface with a roughness length z_0 of 0.05 m) over some areas.⁴ This approach was extended to create extreme wind atlases in different places over the globe when the decades-long, global-coverage reanalysis products became available.^{5,6} Most reanalysis products are of too coarse resolution, both spatially (tens to hundreds of kilometers) and temporally (1 - 6 hours), which do not match the required resolution for the extreme wind as in the IEC standard, which is 10 min. Pryor et al⁷ use directly the 40-year time series of the wind speed at 100 m of the ECMWF Reanalysis data (ERA5) and calculated global atlases of the 50-year wind. The spatial resolution of the ERA5 data is about 30 km, and the data are saved every hour, and the corresponding effective spatial and temporal resolution are even coarser.⁸ The coarse resolution of the model data results in a smoothing effect in the simulated time series and therefore a systematic underestimation of extreme winds.⁹ In recent years, numerical mesoscale modeling at relatively high resolution has become an attractive method for estimating the extreme wind on a global scale. However, these simulations are often challenged with the effective resolution issue too, and at the same time due to the high computational cost, they are usually done for particular regions and often not openly accessible, which makes their output difficult or impossible to assess by engineers in, e.g., under-developed regions.¹⁰

The GASP project uses the latest methods to correct the resolution-related smoothing effect in the numerical modeled time series, and prepare it for microscale modeling, so that the final dataset for the extreme wind is at a spatial resolution of 275 m. At this spatial resolution, the project also uses several approaches to derive other parameters such as the turbulence parameters, flow inclination angle, shear exponent, and air density under extreme wind condition. Based on these siting parameters, we pre-calculate fatigue and extreme loads across the entire globe. By referring these loads with the design loads of the IEC design classes, an atlas is provided with recommended suitable turbine design classes at three heights of 50, 100, and 150 m, with each height using a different turbine model to reflect the sizes of modern wind turbines.

In the following, we will first introduce the various data used in this study for calculations in Section 2. We describe the methods for calculating the long list of parameters in Section 3. Results are shown in Section 4, followed by discussions and conclusions Sections 6 and 7.

2 | DATA

The GASP calculation benefits significantly from several existing data sources such as various reanalysis data and, in particular, from data prepared in the global wind atlas version 3 (GWA3, <https://globalwindatlas.info/>). Sections 2.1 and 2.2 describe these data sources and their use in GASP.

2.1 | Global Wind Atlas data

GWA3 was released in October 2019 and provides a high-resolution atlas of the average wind condition. GWA3 was run for 5 heights (10, 50, 100, 150, and 200 m), at a 275-m resolution, and then interpolated to 9 arc-sec regular latitude/longitude grid. The details of the data and the methods applied to derive them can be found in <https://globalwindatlas.info/about/introduction>.

The calculations in GASP have utilized the following subsets of variables from GWA3: (1) sectorwise variables at 50, 100, and 150 m: Weibull parameters A , k and sector frequency; (2) sectorwise surface variables: mean upwind roughness length, speed-up factors for orography and roughness changes and Ruggedness Index (RIX), which is the percentage of area with slopes exceeding 30° within a 10 km radius; (3) omni-directional mean air density at 50, 100, and 150 m.¹¹

GWA3 prepared the SRTM 3 arc-sec/Viewfinder data set for elevations, which is ready to be used by GASP as input to the high resolution calculations using the microscale model "LINCOM" (Linear Computation Model), developed at DTU Wind Energy Department.^{12,13} The SRTM void-filled 3 arc-sec data (<https://doi.org/10.5066/F7F76B1X>) and the Viewfinder 3 arc-sec DEM (REF) data are both of a spatial resolution of about 90 m. SRTM 3 arc-sec was generally used south of 60°N , with Viewfinder used north of 60°N . However, the Viewfinder data were not fully void-filled so a simple interpolation algorithm was used to fill regions with missing data. In steep terrain, the void-filling algorithm used for SRTM left some artifacts and non-natural looking features, most often Viewfinder had a better result in these regions, so the Viewfinder tiles were used in place of the SRTM data. In the Pacific Ocean, there were several cases of phantom islands in the SRTM data, most likely caused by cloud artifacts and these tiles were also replaced by Viewfinder data. In total, $67 \times 1^\circ$ SRTM tiles were removed and replaced with Viewfinder data.

In connection with the use of the LINCOM model, land cover data were used to estimate the roughness length of the land surface. For consistency with GWA3, GASP uses the same land cover data and roughness translation table, namely the European Space Agency Climate Change Institute Land Cover Classification (ESA CCI-LC) 2015 land cover map (<https://www.esa-landcover-cci.org/?q=node/158>). The ESA CCI-LC dataset was created as part of the CCI program (<https://www.esa-landcover-cci.org/>) to convert MERIS FR (Medium Resolution Imaging Spectrometer Instrument Fine Resolution) surface reflectance mosaics into land cover classes as defined by the United Nations Land Cover Classification System (LCCS). Efforts were made to retain the LCCS classifications of the Globcover 2009 product, however some classes were modified to better describe the land cover class. ESA CCI-LC 2015 has a 10 arc-second (300 m) resolution and was provided in the WGS 1984 coordinate system (EPSG: 4326).

2.2 | The reanalysis data

The GASP project has chosen the Climate Forecast System Reanalysis I (CFSR¹⁴) dataset as the base for the calculation of the extreme winds. These data consists of hourly values from 1979 to 2010, with a spatial resolution of about 40 km. This decision of using CFSR data was made based on comparison with three other reanalysis products: (1) Modern-Era Retrospective analysis for Research and Applications (MERRA)¹⁵; (2) Climate Four-Dimensional Data Assimilation (CFDDA) (<https://cmr.earthdata.nasa.gov/search/concepts/C1214110974-SCIOPS>) and (3) ECMWF Reanalysis 5 (ERA5).¹⁶ The comparison was done on the 50-year wind over Europe and over South Africa, where we have corresponding estimations from measurements for the validation, e.g., Hansen et al¹⁷ and Larsén and Kruger.¹⁸

Results of the comparison suggest that the spatial distribution of the 50-year wind at $z=10$ m differs in one reanalysis product from another, particularly over land. Results from CFSR and MERRA are comparable and are in better agreement with measurements in South Africa than CFDDA and ERA5. The best estimate results from using CFSR for South Africa, which has also been reported earlier in the study of Larsén and Kruger (2014)¹⁸ comparing with measurements from more than 70 stations. Both CFDDA and ERA5 significantly underestimate the winds over South Africa (see details in Larsén et al.¹⁹)

3 | METHODS

Calculations in the GASP project consisted of two phases, the first involved downscaling atmospheric data to estimate the necessary meteorological parameters used in site assessment, while the second consisted of using that data to perform load estimates and provide maps of the recommended turbine class. Both of these are presented on a global 9 arc-sec latitude-longitude grid, approximate 275 m. In this section, we first introduce the global calculation system and then the methods for the key parameters including flow inclination angle, shear exponent, air density for extreme wind conditions, extreme wind, turbulence intensity and load.

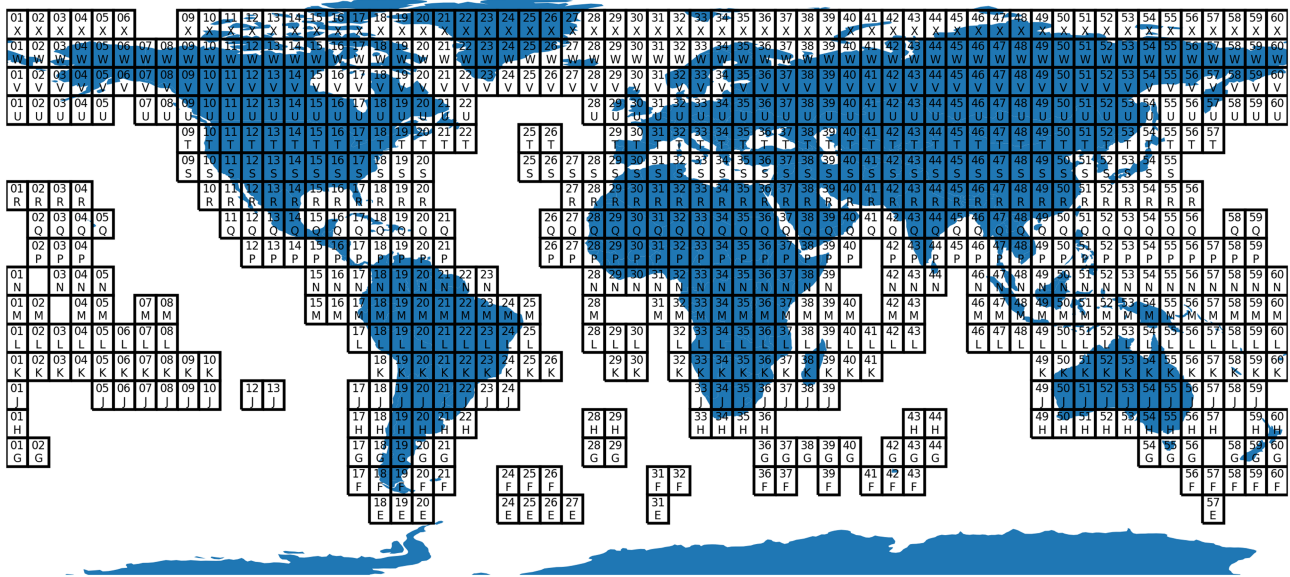


FIGURE 1 The GASP run tiles used to distribute the calculation tasks. Each tile has a size of $6^\circ \times 8^\circ$. Only tiles between 85°N and 60°S that include an area within 200 km of a coastline are included

3.1 | The global calculation

The global GASP calculations cover between 85°N and 60°S . Following GWA3, over water, only for areas within 200 km from the shorelines the values are re-gridded to grid size of 275 m. The global land mask used to identify which locations should be simulated, was created by buffering the Global Self-consistent, Hierarchical, High-resolution Geography Database.²⁰ GSHHG

The calculation uses the Universal Transverse Mercator (UTM) projection, which required a tiling system of the globe. The tiling system splits the globe into $6^\circ \times 8^\circ$ run “tiles” that are named according to a two-digit numeric column identifier, corresponding to the UTM “zone”, and a single letter row identifier. Figure 1 shows the location of the 751 run tiles used in GASP. The orographic and landcover data were clipped for each run tile. Additionally a calculation mask was made for each tile using the GSHHG fine resolution dataset with a 200 km buffer in the UTM projection of each tile.

For each run tile, a number of calculation tiles were defined in the corresponding UTM projection, which were used to carry out the raster based LINCOM simulations. Each calculation tile has 800×800 grid points with a spacing of 125 m, and an overlap with the neighboring grid edges. For each calculation tile, the topographic data are clipped with a 15 km buffer and re-projected to the 125 m UTM grid using the nearest neighbor interpolation method. This interpolation was required for the land cover due to the discrete nature of the variable.

3.2 | A list of variables for calculating the siting parameters

Here we explain how to obtain a list of variables that are further used for calculating the extreme wind, turbulence and load: shear exponent, terrain complexity and air density for extreme winds.

LINCOM uses raster maps of roughness and orography in a meter-based map projection in the grid tiling system (section 3.1). LINCOM was run using a uniform wind speed of 10 m s^{-1} over the domain at 10 m with a roughness length $z_0 = 0.05 \text{ m}$, to obtain the wind at 50, 100, 150, and 200 m above the surface. The results are first interpolated from the 125 m grid to 9 arc-sec locations using bi-linear interpolation for the flow inclination angle and wind speed and using nearest neighbor for z_0 . The wind speed at various heights was then used to find the shear exponent; we used heights of 50 and 100 m for the 50 m output height; 50, 100, and 150 m for the 100 m height; and 100, 150, and 200 m for the 150 m height. The quasi-linear model LINCOM is only weakly sensitive to the input wind regarding the calculation of the shear exponent.¹² In GASP, the shear exponent is used in one of the two methods for turbulence calculation (Section 3.4.2).

The terrain complexity is relevant for the load calculations. It is defined in the IEC standard² based on the calculation of the slope and variation of orography data. We used the GWA3 elevation data for the calculation, which is of an approximate spatial resolution of 90 m, but interpolated to 50 m using cubic interpolation, and re-projected to the UTM projection of the grid, in order to match the standard recommendation of 50 m.

To better estimate the loads at high wind speeds, the air density for the highest 2% of winds ($\rho_{50,site}$) was calculated. We calculated the necessary variables, the pressure P , temperature T , and water vapor from hourly ERA5 reanalysis data in the same way as described in Floors et al.,¹¹ but using the 0.98 percentile of highest winds over the period 2010–2020. The air density was then calculated for each height using the three variables. More information about this procedure can be found in Larsén et al.¹⁹

3.3 | Siting parameter: the 50-year wind

The calculation of the 50-year wind involves a chain of models downscaling the reanalysis data (Section 2.2) to a local scale with a grid spacing of about 275 m at the site, as explained in Sections 3.3.1 to 3.3.3.

3.3.1 | The modeling chain

The modeling chain is illustrated in Figure 2. We start from the CFSR wind components at 10 m (longitudinal U_{10} and meridional V_{10}). For tiles covering land (upper arrow-flow in Figure 2), the data will then go through the so-called generalization process (details in section 3.3.2) and be converted to wind of the “standard condition” (U_{ST}) over a homogeneous surface at $z=10$ m with $z_0=0.05$ m. The spectral correction method (section 3.3.3) will then be applied to convert the generalized winds to an equivalent temporal resolution of 10 min (U_{st}). The microscale flow model LINCOM then uses U_{st} as input to obtain the site-specific wind at a spatial grid spacing of 275 m with an equivalent temporal resolution of 10 min. For tiles covering water only (lower arrow-flow in Figure 2), no generalization nor LINCOM downscaling but the spectral correction is applied to obtain the wind at the same spatial grid spacing as the reanalysis but a temporal resolution of 10 min. Based on the tropical cyclone tracks where the track density is highest, we marked these areas as “tropical cyclone affected areas” and for them, the spectral correction method is applied with calibration with best track data; see also section 3.3.3.¹⁹ Note that such a selection of tropical cyclone areas does not include all areas with presence of tropical cyclones.

3.3.2 | Generalization of the reanalysis data

The purpose of converting the reanalysis wind to a generalized condition, namely, 10 m over a homogeneous surface with a roughness length of 0.05 m is to prepare the data for downscaling the wind to local condition through the microscale LINCOM model (upper arrow-flow in Figure 2).

This is a concept used in DTU's software WAsP and WEng. Usually, we use measurements from a meteorological mast close to the turbine site and “clean” the wind data by removing the local speedup effects from orography and roughness changes around the mast and then convert them to the geostrophic wind G through the geostrophic drag law (step 1). At step 2, by assuming the same G over both the measurement site and the turbine site, a reverse process to step 1 is applied with a new roughness length of 0.05 m to obtain the standard wind (U_{st}) at the turbine site. With U_{st} as input, the local effects around the turbine site are calculated by the microscale modeling, and the wind at the turbine site is obtained. Details of this process can be found in, e.g., Troen and Petersen²¹ and Badger et al.²²

In the absence of measurements, in GASP, we use reanalysis wind data. The reanalysis data have a spatial grid spacing of tens of kilometers, with the turbine site in the grid space. It is therefore reasonable to combine steps 1 and 2 as mentioned previously to generalize the reanalysis wind to the standard condition U_{st} , which is then ready to be used in the microscale modeling. We first apply the LINCOM model to the reanalysis

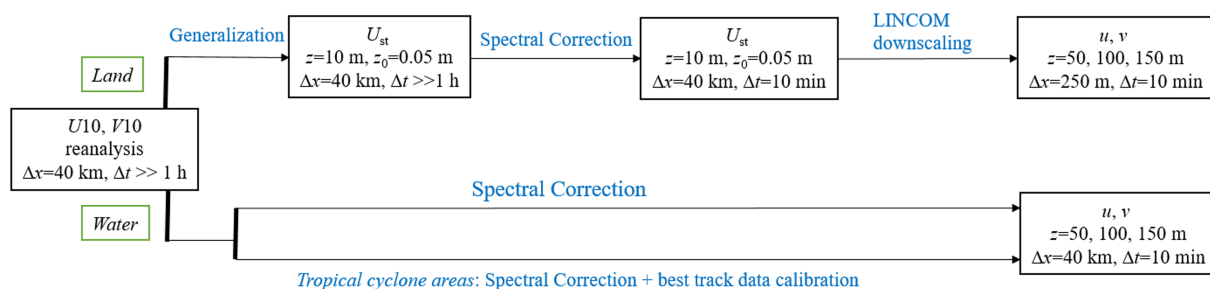


FIGURE 2 The model chain for downscaling the wind from reanalysis (with spatial resolution Δx about 40 km and temporal resolution Δt lower than 1 h) to the local condition ($\Delta x = 275$ m and $\Delta t = 10$ min), for land and water grids, respectively

orography and roughness length z_0 to obtain the speedup effect in 36 directional sectors s_o and s_r , respectively. Here, z_0 is obtained from reanalysis wind U at 10 m and the corresponding friction velocity through the logarithmic wind law for the surface layer:

$$z_0 = z \cdot \exp(-\kappa U(z)/u_*), \quad (1)$$

where $z = 10$ m. The “cleaned” wind speed is obtained following the method in Troen and Petersen,²¹ and the corresponding friction velocity is obtained using Equation (1), so that it can be used in the geostrophic drag law to obtain G . With G and a new roughness length of $z_0 = 0.05$ m, we obtain a new friction velocity through Equation (2):

$$G = \frac{u_*}{\kappa} \sqrt{\left(\ln \frac{u_*}{f_c z_0} - A\right)^2 + B^2}, \quad (2)$$

where f_c is the Coriolis parameter and A and B are dimensionless parameters, which are $A = 1.8$ and $B = 4.5$ in Landberg et al.²³ Applying Equation (1) with $z_0 = 0.05$ m and new friction velocity, we obtain the generalized wind U_{st} for 36 directional sectors.

The above process is applied to land grid points to prepare the “regional extreme wind,” which has the same spatial and temporal resolution as the reanalysis data. Once it undergoes the spectral correction (Section 3.3.3), it is ready to be used as forcing to the microscale LINCOM model.^{12,24}

3.3.3 | The spectral correction method

The spectral correction method was developed by Larsén et al.⁹ to fill in the missing wind variability in numerically modeled time series of wind speed. Time series of wind speed from numerical models are often smeared in comparison with measurements of the same temporal interval, as a result of the diffusion function in the model that is used to ensure numerical stability for the calculations in a model. This is reflected as low spectral energy in relevant frequencies. This missing wind variability at relatively high frequencies is particularly important for the calculation of extreme wind of 10-min averages. Such an effect on the calculation of the extreme wind is estimated in Larsén et al.⁹ assuming that the once-per-year exceedance follows a Poisson process. With a large threshold, such a distribution of the exceedance can be simplified as a Gaussian process. The maximum wind that occurs once a year \bar{U}_{max} was derived as a function of the zero- and second-order spectral moments m_0 and m_2 :

$$\bar{U}_{max} = \bar{U} + \sqrt{m_0} \sqrt{2 \ln \left(\frac{1}{2\pi} \sqrt{\frac{m_2}{m_0}} T_0 \right)}, \quad (3)$$

where \bar{U} is the mean wind speed, T_0 is the basis period of one year, and m_i is the i th spectral moment defined by

$$m_i = 2 \int_0^{\infty} f^i S(f) df, \quad (4)$$

where f is the frequency in Hz and $S(f)$ is the spectrum of the wind speed. One can see that \bar{U}_{max} is significantly affected by m_2 . Thus, if we can fix the spectral tail, we improve the calculation of \bar{U}_{max} .

In Hansen et al.,¹⁷ the information of the tails is provided by 10-min time series of measurement of relatively short length, e.g., 1 year. Such a length is often not a problem at most campaigns for wind siting.

In Larsén and Kruger,¹⁸ the information of the tails is provided by a spectral model:

$$S(f) = n_1 \cdot a \cdot f^{-5/3}, \quad (5)$$

which is mesoscale part of the expression from Larsén et al.²⁵ for $(1 \text{ day})^{-1} < f < 10^{-3}$ Hz, with n_1 a coefficient that is affected by weather types or height above the surface; n_1 can be adjusted with measurements or available spectrum of adjacent frequency ranges.

For the global calculation in GASP, as measurements are in general not available, we use Equation (5) to correct the spectrum obtained from the reanalysis data. When applying Equation (5), we need to define two frequency parameters, a start frequency f_c and an end frequency f_h . f_h refers to the highest frequency which is related to the resolution in target, e.g. if we want to correct the spectrum to 10-min resolution, $f_h = 72 \text{ day}^{-1}$, which is the Nyquist frequency corresponding to a 10-min time series. f_c is the frequency where we start replacing the spectrum from the original spectrum. Here we use $f_c = 0.8 \text{ day}^{-1}$ as the default frequency value, see Figure 3. In areas where convective conditions are

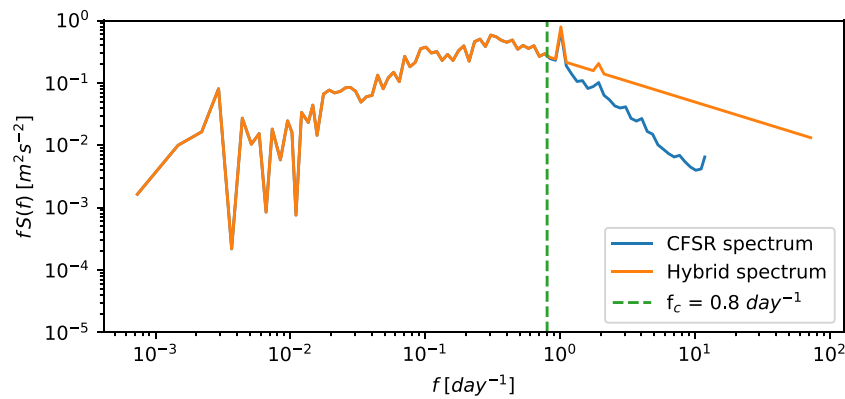


FIGURE 3 The spectrum of a 5-year CFSR wind speed time series and the corresponding hybrid spectrum at a random grid point in North America. The hybrid spectrum is corrected for $f > 0.8 \text{ day}^{-1}$

frequently observed, using $f_c = 0.8 \text{ day}^{-1}$ can result in a hybrid spectrum with lower energy content than the corresponding CFSR spectrum for frequencies $f_c < f < 5 \text{ day}^{-1}$. To avoid this problem, two additional values, 1.3 and 2.2 day^{-1} , were used as f_c . These values are slightly larger than the diurnal and half-diurnal peaks respectively. Further, we define three corresponding test frequencies $f_t = (1.0, 1.5, 2.5) \text{ day}^{-1}$. If $S(1.0)_{\text{hybrid}} > S(1.0)_{\text{CFSR}}$, the first value of f_c is kept. Otherwise, we use the next value of f_c and repeat the test with the second value of f_t , and so on.

By default, $n_1 = 1$ in Equation (5); for tropical cyclone affected area, $n_1 \geq 1$, which is obtained as a function of wind speed, as calibrated using the Best Track data from Ott²⁶ and the estimation from CFSR data; Larsén and Ott.²⁷

Thus, the correction factor can be obtained as the ratio of U_{max} using the corrected, hybrid spectrum (orange curve in Figure 3) over the original spectrum (blue curve in Figure 3), denoted as $\bar{U}_{\text{max}}^{\text{hybrid}}$ and $\bar{U}_{\text{max}}^{\text{uncorr}}$, respectively, through Equation (3):

$$r_{\text{sc}} = \frac{\bar{U}_{\text{max}}^{\text{hybrid}}}{\bar{U}_{\text{max}}^{\text{uncorr}}} \quad (6)$$

r_{sc} is used to correct the annual maximum winds extracted directly from the reanalysis data.

3.3.4 | Downscaling extreme winds and calculating V50

For each reanalysis data grid over land, the generalization (Section 3.3.2) and spectral correction method (Section 3.3.3) were used to obtain annual maximum winds in 12 directional sectors. As shown in Figure 2, to obtain V50, the next step is to use the LINCOM model to downscale the winds to the specific local conditions at each output location. In the downscaling procedure, LINCOM is used as described in Section 3.2, with three generalized wind forcing levels at 10 , 25 , and 40 m s^{-1} . From the LINCOM downscaling, a lookup table is generated for each output grid point with 275 m grid spacing mapping the relationship between the generalized wind and the “actual” local wind at the three output heights 50 , 100 , and 150 m . This lookup table is used together with the spectrally corrected, generalized wind from the reanalysis data to provide the corresponding local wind in 12 direction sectors. Following this, the maximum directional wind speed is selected from each year, which forms 32 samples for each 275 m -grid, at the three heights. To obtain the corresponding 50-year wind, we use the Annual Maximum Method, together with Gumbel distribution.

In GASP, over water, there is no high-resolution calculation using the microscale LINCOM model. Instead, we calculate the extreme wind from one height to another, through the logarithmic wind law:

$$U_z = (u_* / \kappa) \ln(z/z_0). \quad (7)$$

With U_{10m} at $z = 10 \text{ m}$ known, if we derive one more equation for z_0 and u_* , we can obtain U_z analytically.

We tested three approaches for obtaining the relation between z_0 and u_* : the Charnock formulation,²⁸ the algorithms from Andreas et al,²⁹ and the formulations from the SWAN model.³⁰ The 10-m wind speed in the range from 1 to 40 m s^{-1} was extrapolated to 100 m using the three approaches, and the results were compared. The results for the three methods were nearly identical for winds up to 25 m s^{-1} . The wind speeds from the SWAN formulations are about 2 m s^{-1} smaller than the other two methods at a speed of 50 m s^{-1} . We choose the SWAN formulation

for the final calculation, as it provides a saturation of surface drag or roughness length at strong winds, which is often interpreted as related to the wave breaking processes:

$$\begin{aligned} C_d &= (0.55 + 2.97(U_{10m}/31.5) - 1.49(U_{10m}/31.5)^2)10^{-3}, \\ u_* &= \sqrt{C_d}U_{10m}, \\ z_0 &= 10\exp(-\kappa U_{10m}/u_*). \end{aligned} \quad (8)$$

3.3.5 | Merging offshore and onshore results for the 50-year wind

As shown in Figure 2, two methods were used for land and water points, respectively. A correction strategy for coastal sites was therefore introduced to mitigate emerging unrealistic speed-ups from water to land near the coast when offshore and onshore results are combined. For this purpose, offshore data derived from the spectral corrected CFSR data were extrapolated further inland by means of the ‘‘Creep filling’’ technique provided by the Earth System Modeling Framework.³¹ We used the creep-filled data to replace the extreme wind estimates from LINCOM at onshore coastal sites at all locations that fulfill the following three conditions: The location lies on land with a distance ≤ 50 km to a coastline; the terrain elevation is below 500 m, and LINCOMs extreme wind is higher than the extreme wind estimate obtained from creep-filled data would suggest.

3.4 | Siting parameter: The turbulence

For GASP, the distribution of turbulence intensity (TI) was calculated as a function of wind speed. The definition of TI is

$$TI = \sigma_u / U, \quad (9)$$

where U is the mean wind speed and σ_u is the standard deviation of the along-wind component of the wind vector during a period τ . The variance of the along-wind component is similar to that of the wind speed. For typical boundary-layer flow, τ is in the range of 10 min to 1 h.

To the IEC standards, a linear regression is done between the TI and wind speed; thus, a pair of coefficients a and b are obtained as in

$$TI = a \cdot U + b. \quad (10)$$

In connection with the application in the IEC standard, it is also required to obtain the coefficients for the distribution of σ_{σ_u} with the wind speed:

$$\sigma_{\sigma_u} = a_\sigma \cdot U + b_\sigma. \quad (11)$$

Two approaches are used for calculating TI over land. Approach 1 uses the typical boundary layer turbulence model, the Kaimal model,³² using input of surface roughness lengths (Section 3.4.1). Approach 2 is through terrain-affected shear and a stability correction, based on the turbulent kinetic energy (TKE) budget (Section 3.4.2). Over water, only approach 1 is used.

The two approaches were validated through blind tests using measurements from more than 10 stations globally, and it is found that the ensemble, namely the average of the two, provides least bias. The final data of turbulence are therefore produced using the ensemble.

3.4.1 | Turbulence via the Kaimal spectrum

With this approach, we calculate σ_u as the root-mean-square of the integrated power spectrum of u for a range of wind speeds from 1 to 50 ms^{-1} , with $z = 50, 100,$ and 150 m. Here, we use the Kaimal spectral model³² for u , Equation (12):

$$fS_u(f) = \frac{102u_*^2 n}{(1 + 33n)^{5/3}}, \quad (12)$$

where n is the normalized frequency $n = fz/U$. The integration is applied over the frequency f from 1 h^{-1} to 10 Hz.

An important input is z_0 at a spatial resolution of 275 m, which will be used to obtain u_* for application in Equations (12) through (7).

For an offshore site, z_0 is calculated using Equation (8). For an onshore site, z_0 is obtained from the GWA3 dataset: It contains 12 sector-wise roughness values, each obtained by a weighted average of upwind roughness length.³³ For each site, a wind-direction sector frequency-weighted value is obtained for z_0 . This sector frequency for each grid point of 275 m spacing is also provided by the GWA3 data (see Section 2.1). When calculating the σ_{σ_u} , T was calculated for each sector, and a collection of σ_u is then generated with the given occurrence-frequency in that sector; thus, the calculation of standard deviation of σ_u can be done. Coefficients a and b were obtained from a linear fit of T with U (Equation 10), and a_σ and b_σ from a linear fit of σ_{σ_u} with U (Equation 11) in the range 5–20 ms^{-1} , as well as 10–30 ms^{-1} .

Approach 1 applies the assumption of neutral stability, as stability data are not available. It does not seem immediately suffer from this assumption.

3.4.2 | Turbulence via kinetic energy budget with terrain effects

In Approach 2, a model has been derived to get mean σ_u as affected by stability and rooted in shear production. Following Kelly et al,³⁴ it can be seen as an extension of local-similarity theory (consistent with, e.g., Nieuwstadt³⁵), plus terrain-induced turbulent transport.³⁶ Its equation for the “strength” of along-wind fluctuations averaged over all speeds (and conditions) is

$$\langle \sigma_u \rangle = \frac{\langle \alpha \rangle \langle U \rangle + T}{1 + z L_{\text{eff}}^{-1}}, \quad (13)$$

where the brackets correspond to long-term means, with α being the shear exponent ($d \ln U / d \ln z$), T being the turbulent transport contribution due to inhomogeneous terrain, and L_{eff}^{-1} being the effective mean stability (reciprocal of Obukhov length). These can be calculated using binned L^{-1} values from e.g. mesoscale data and in situations when such mesoscale data are not available or reliable, it was necessary to find a representative “default” global stability, as done in standard WAsP usage.^{21,37} Introducing this global stability also improves the calculation in connection with Approach 2.

While L_{eff}^{-1} is ideally comprised of contributions from the standard deviations (and mean) of L^{-1} , here lacking this information we use $L_{\text{eff}}^{-1} = 0.01 \text{m}^{-1}$ following Kelly and Troen³⁷; more details may be found in Kelly.³⁸ We note that LINCOM, which provides the α used in (13), calculates assuming neutral conditions. Thus the shear must be compensated; this is done using $\alpha = \alpha_N \Phi_m(z L_{\text{eff}}^{-1}) / [1 - \alpha_N \Psi_m(z L_{\text{eff}}^{-1})] = \alpha_N (1 + 5z L_{\text{eff}}^{-1}) / [1 + 5\alpha_N z L_{\text{eff}}^{-1}]$, following from Kelly et al³⁹ and amenable to perturbed flow above the surface layer.³⁴ Here Φ_m and Ψ_m are the Monin-Obukhov correction functions for mean shear and wind speed, respectively, and α_N denotes the neutral shear output from the microscale model.

Terrain-induced turbulence is represented by the horizontal turbulent-transport term (T) of the dimensionless TKE budget. To conform to the IEC 61400-1 prescription, in Equation (13) T is parameterized such that it can be cast as a factor multiplying $\langle \alpha \rangle \langle U \rangle$; expressed as a multiplier of the main part ($\langle \alpha \rangle \langle U \rangle$), the terrain-complexity component of T can range between 1 and 1.4, thus offering 15% increase per the IEC, with partial safety factor of 1.2. Two crude empirical forms for sector-wise terrain-enhancement (T) are given: one based on directional RIX, and the other based on terrain-inclination angle (η). Both also have a common z_0 -dependence, to account for the turbulence augmentation due to forest, etc. The forms employed are $T(\eta) / (\langle \alpha \rangle \langle U \rangle) = 0.4 \tanh(4\eta) f_R(z_0)$ and $T(\text{RIX}) / (\langle \alpha \rangle \langle U \rangle) = 0.4 \tanh(\text{RIX} / \text{RIX}_{\text{ref}}) f_R(z_0)$, where $\text{RIX}_{\text{ref}} = 0.1$ (i.e., 10%) and the roughness dependence $f_R = [1 + \ln(\max\{z_0/z_{0,\text{ref}}, 1\})]^{0.1}$ accounts for stronger turbulence found over very rough terrain, such as forest (with $z_{0,\text{ref}} = 0.1 \text{m}$ being the roughness at which enhancement begins).

To conform with 6.3.2.3 of the IEC 61400-1 standard, we parameterize a linear dependence of σ_u on U ,

$$\sigma_u = \left[\frac{c_\sigma \langle \sigma_u \rangle + d_\sigma}{\langle U \rangle} \right] U + [\langle \sigma_u \rangle (1 - c_\sigma) - d_\sigma], \quad (14)$$

where $\langle \sigma_u \rangle$ is calculated by Equation (13) and $\langle U \rangle$ is from GWA3. The parameters $c_\sigma = 0.1$ and $d_\sigma = 0.75 \text{m s}^{-1}$ were obtained by fitting to data with the IEC form as baseline (though they could presumably vary between 0 and 1); one sees that when $U = \langle U \rangle$ then $\sigma_u = \langle \sigma_u \rangle$.

Further, an estimate of the 90th percentile of turbulence is made, using $\langle \sigma_u \rangle$ from Equation (13):

$$\langle \sigma_{u90\%} \rangle \approx (C_{90} \langle \sigma_u \rangle)^{x(z_0)}, \quad (15)$$

where a slight roughness dependence comes via the parameter

$$x(z_0) \equiv 1 - c_1 \{1 + \tanh[\ln(z_0/z_{0,\text{ref}})]\} \quad (16)$$

amenable to either the log-normal or Weibull forms in edition 3 or 4 of the IEC 61400-1. The x parameter accounts for change in width of the distribution of σ_u over very rough surfaces and is made to be consistent with $f_R(z_0)$ in T ; it varies from 1 for typical roughnesses down to ~ 0.8 over forest. In Equation (15), the constants $c_1 = 0.1$ and $C_{90} = 2$ were chosen empirically based on the IEC guidance. A simple extension is made to include the U -dependence, consistent with (and using) the roughness-dependence in $\langle \sigma_{u90} \rangle$ above:

$$\sigma_{u90\%}(U) \approx \langle \sigma_{u90\%} \rangle [1 + c_{A90}(U/\langle U \rangle - 1)] \quad (17)$$

using $c_{A90} = 0.7$.

3.5 | Calculation of the turbine class

3.5.1 | Wind turbine classes and design load cases

The IEC 64100-1 standard includes design requirements calculated according to individual design load cases (DLCs). Each individual DLC treats an expected state of the wind turbine during its lifetime with one or more external conditions; this can be e.g. an operational or shut-down state, under normal wind conditions or various extreme events. In general, the DLCs are divided into two groups: ultimate limit state analysis (ULS) that covers extreme wind conditions, and fatigue limit state analysis (FLS) that covers typical wind conditions. ULS and FLS are equally important to ensure structural integrity of wind turbines over their lifetime, hence, both are considered in the GASP project.

The workflow from siting parameters, to inputs of site climate and site loads, to the site design class is illustrated in Figure 4, where the site conditions (upper workflow with red arrows) are compared with design conditions (lower workflow with green arrows).

3.5.2 | Extreme load (ULS) estimation

To calculate a global map of extreme loads, DLC 6.1 from the IEC 61400-1 standard is considered; this addresses parked turbines experiencing a 50-year extreme wind. Assuming that extreme loads increase monotonically with increasing wind speed and air density, the ultimate limit state is considered satisfied (not exceeded) if it can be shown that the site-specific extreme wind conditions are more benign than the design class conditions, according to

$$\rho_{\text{design}} V_{\text{ref}}^2 \geq \rho_{50,\text{site}} V_{50}^2. \quad (18)$$

Using the previously calculated site-specific extreme air density $\rho_{50,\text{site}}$ (Section 3.2) and extreme wind speed at hub height V_{50} (Section 4), Equation (18) has been examined globally for determining wind turbine classes I, II, III, and Tropical (see Table 1).

3.5.3 | Fatigue load (FLS) estimation

The fatigue limit state is examined in accordance with the IEC 61400-1 design standard design load case 1.2, which covers fatigue loads during normal operation of turbines. To significantly speed up calculations, a response surface methodology has been used to calculate the fatigue loads.

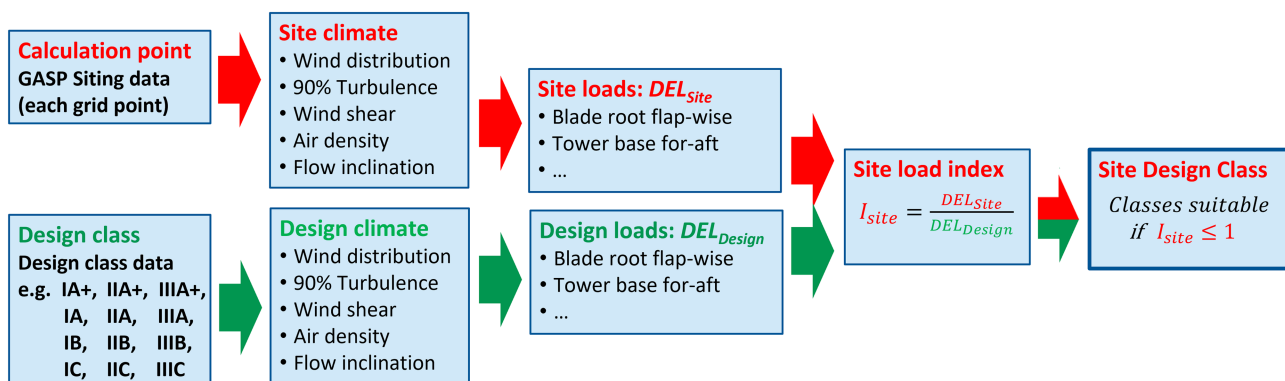


FIGURE 4 Workflow from GASP siting parameters to site design class, with site conditions (red arrows) in comparison with design standards (green arrow)

TABLE 2 Wind turbine components

Components	Description	Notation	Type	Wöhler exponent
Blades	Blade root flap-wise bending	RootMyb1	DEL	10
Drive train	Low speed shaft torque	LSSGagMxa	LDD	6
Nacelle	Yaw bearing tilt	YawBrMyp	DEL	4
Tower	Tower bottom fore-aft bending	TwrBsMyt	DEL	4

This is based on a multiple linear regression surrogate model, calibrated by pre-simulated loads using a central composite experimental design; its theoretical background is covered extensively in Toft et al.⁴⁰ which also quantifies and validates its accuracy for current purpose of estimating fatigue loads across a wide range of characteristic wind climates. When site-specific fatigue loads are calculated, they are compared to the design class loads, and a recommendation is made by identifying the turbine design class which is closest to the site-specific load, i.e., the design class with the lowest fatigue load margin is recommended accordingly. All design classes that are listed in Table 1 have been considered, from 1A+ to 3C.

To provide accurate turbine class recommendations it is essential that representative turbine models are considered for each height, here 50, 100, and 150 m. Load response models are accordingly prepared for three generic turbine models in this project: the 1.5 MW WindPACT turbine⁴¹ for 50 m hub height, the 5MW reference wind turbine by NREL⁴² for 100 m, and the 10MW reference wind turbine by DTU⁴³ for 150 m. Each model is simulated in the aero-servo-elastic code FAST.⁴⁴ Subsequently, fatigue loads are estimated on the set of load bearing components outlined in Table 2. The fatigue strength of each component is modeled by typical Wöhler exponents (m) used for welded steel details ($m = 4$), cast steel details ($m = 6$) and blade composite materials ($m = 10$). Collectively, the chosen components represent the overall “path” of the wind loads, starting from wind input acting on the blades, through the turbine system and the reaction of the foundation; they cover varying sensitivities towards the dominant input wind climate parameters.

3.5.4 | Wake effects

Nowadays wind turbines are usually installed within a wind farm, where each turbine can shed a wake on neighbouring turbines. The wakes increase the turbulence levels, which in turn increase fatigue loads and damage. To realistically account for wake effects, the GASP project adopts a standard grid-layout, with a spacing of 5 rotor diameters (RD) between turbines in the main wind direction, and a 3 RD spacing in the horizontal direction perpendicular to the main direction. This allows for calculation of an atlas of expected design class both with and without wake effects. The total turbulence level is assessed by summing the squares of ambient and wake-related turbulence, i.e.,

$$\sigma_{U,total}(U,\theta) = [\sigma_{U,c}^2(U,\theta) + \sigma_{U,wake}^2(U,\theta)]^{1/2}; \quad (19)$$

here, $\sigma_{U,c}$ is the ambient turbulence contribution, θ is the direction, and $\sigma_{U,wake}$ models the wake-added turbulence according to the IEC 61400-1 standard:

$$\sigma_{U,wake}(U,\theta) = \frac{U}{1.5 + 0.8RD(\theta)/\sqrt{C_T(U)}}, \quad (20)$$

with C_T the turbine specific thrust coefficient.

3.6 | Uncertainty classification

A method was developed to assess uncertainties in two key parameters: the 50-year wind and the turbulence intensity.

Rather than the more standard probability assessment or quantification, the classification of uncertainty here employs a “traffic-light” principle for the following reasons: (1) GASP has a complicated calculation system, including a chain of calculations. Each step of the chain has a list of methods with associated assumptions; (2) There are a large number of different data sources for each step of the calculation. The data quality of each data source are different; (3) At a spatial resolution of 275 m, a global assessment of the sensitivity tests with the above mentioned

methods and data, the calculation is too big for the scope of this work; (4) There are no sufficient reference data such as measurements for a global assessment of the absolute uncertainty.

The detailed algorithms can be found in Larsén et al.⁴⁵ Briefly, the assessment of uncertainties follows the data (section 2) and methodologies (section 3) that are used for the calculation of the two parameters. We first classify each grid cell into one of 16 categories depending on whether it is land or sea (through land use data), the complexity of terrain (through RIX number), the complexity of roughness length change in space (through speedup factor due to roughness length change) and whether it is a coastal area or not (through distance to shoreline), and whether it is within the predefined “cyclone-affected” areas (predefined area through latitude and longitude). For each category, the list of parameters used for their corresponding calculations are assigned a number between 1 and 3, with 1 suggesting good reliability of the input data quality and 3 suggesting high uncertainty. The respective contributions from the list of parameters are weighted based on qualitatively assessed sensitivity tests. Thus, the output is a weighted number we call the “uncertainty class index,” between 1 and 3, with 1 suggesting that the calculation is reliable and 3 not reliable. For the 50-year wind, we used indices 1–1.6 for green, 1.6–2.5 for yellow, and 2.5–3 for red. For the turbulence, we used indices 1–1.5 for green, 1.5–2.5 for yellow, and 2.5–3 for red. These indices for assigning colors, and hence grouping the data, are found using simple clustering algorithms, separately for U_{50} and TI , respectively, as explained in Larsén et al.⁴⁵

4 | RESULTS

The calculated layers of atlas parameters are presented on the open data portal <https://science.globalwindatlas.info/#/map>.⁴⁶ Parameters include “Turbine Class” (ULS, FLS No Wake and FLS with Wake classes), “Atmospheric Variables” (U_{50} , Turbulence Intensity and Shear exponent), “Uncertainty Classification” (U_{50} and Turbulence Intensity) and “Orographic Variables” (Terrain complexity and Flow inclination angle).

In the following, we briefly introduce the results of the 50-year wind, turbulence intensity, uncertainty classification, and turbine classes.

The global atlas of the 50-year winds are created at three heights: 50, 100, and 150 m. Values at other heights can be obtained by applying a specific fitting to the values at the three heights. The atlas includes the 50-year winds over land at a spatial resolution of 275 m. Over water, the spatial resolution is the same as the reanalysis data, here the CFSR data, namely, about 40 km, but interpolated to spatial grids of 275 m. Both correspond to 10-min temporal resolution as a result of the spectral correction (Section 3.3.3). Figure 5 shows an example of the 50-year wind at 100 m, in a similar manner to the existing global wind atlas (GWA) dataset (www.globalwindatlas.info), including all land surfaces and water areas within 200 km from the coastline.

The turbulence models are used to calculate distributions of the standard deviation of the wind speed σ_U , as well as turbulence intensity TI . Quantities such as standard deviation of σ_U , and its distribution with wind speed and the regression functions are also derived. They are used as input to calculate extreme and fatigue loads. Figure 6 shows an example of the one global data layer, the average turbulence intensity at 100 m. The turbulence data are also available at three heights of 50, 100, and 150 m, with the same grid spacing as for the extreme wind.

Results for the expected design classes are split into extreme wind design class (ULS) and fatigue design classes (FLS). FLS is further split into results with and without wake effects. When the limits for all standard design classes are exceeded, customized design classes are required. This category of design classes, where the designer specifies the custom design requirements, is referred to as “Class S.”² The results for ULS and FLS are first presented as a global overview visualizing the classes in Figures 7 and 8, respectively. The respective statistics of the distribution among the different design classes are summarized in Tables 3 and 4. Note that the global statistics are based on data over areas shown in Figures 7 and 8, namely, excluding open waters 200 km away from the shoreline and outside 85°N to 60°S.

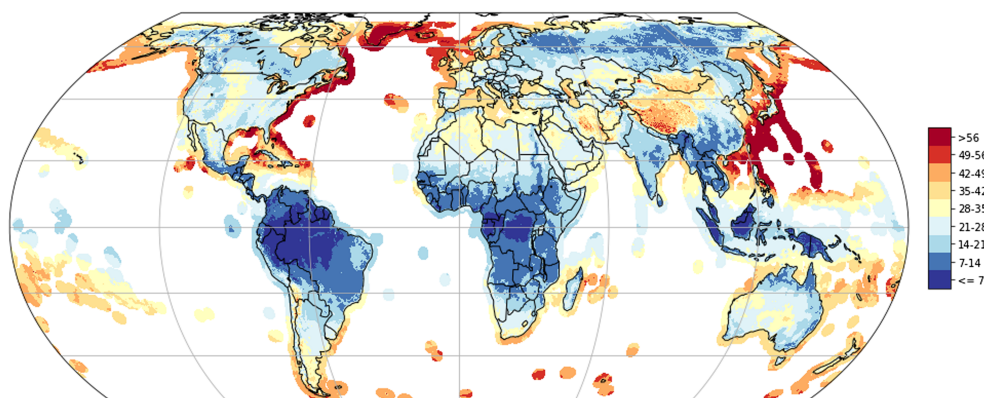


FIGURE 5 The 50-year wind at 100 m at a spatial resolution of 275 m, over all land and water (200 km from coastline)

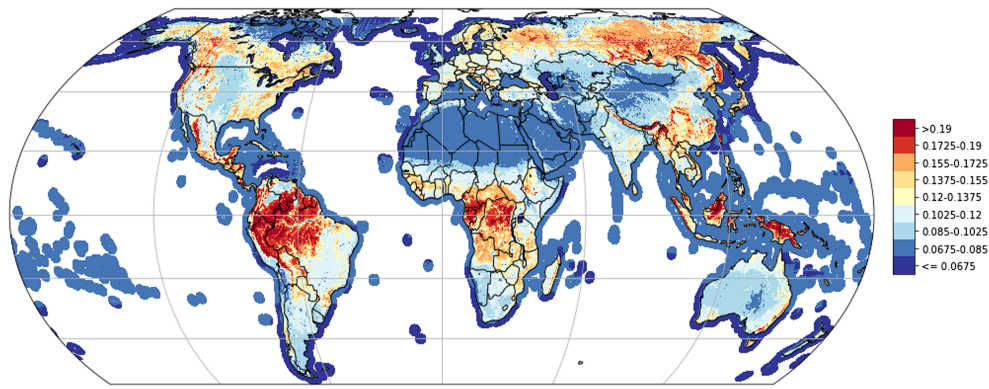


FIGURE 6 The averaged turbulence intensity at 100 m at a spatial resolution of 275 m, over all land and water (200 km from coastline)

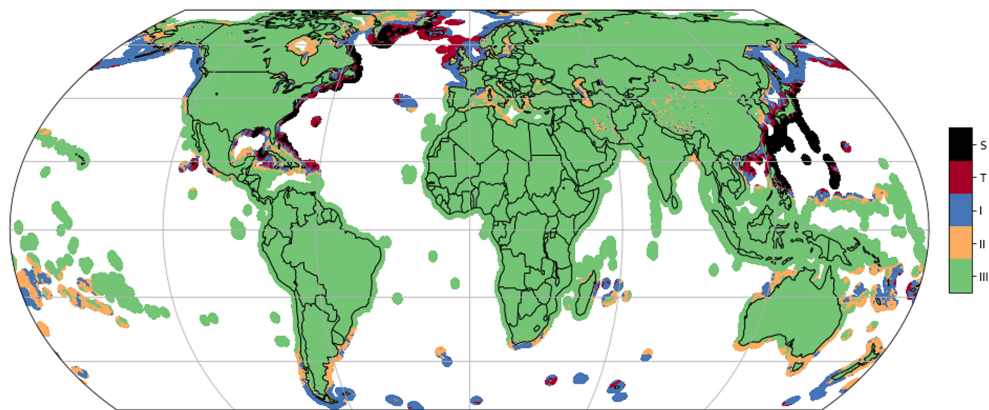


FIGURE 7 The ULS design classes at 100 m at a spatial resolution of 275 m, over all land and water (200 km from coastline)

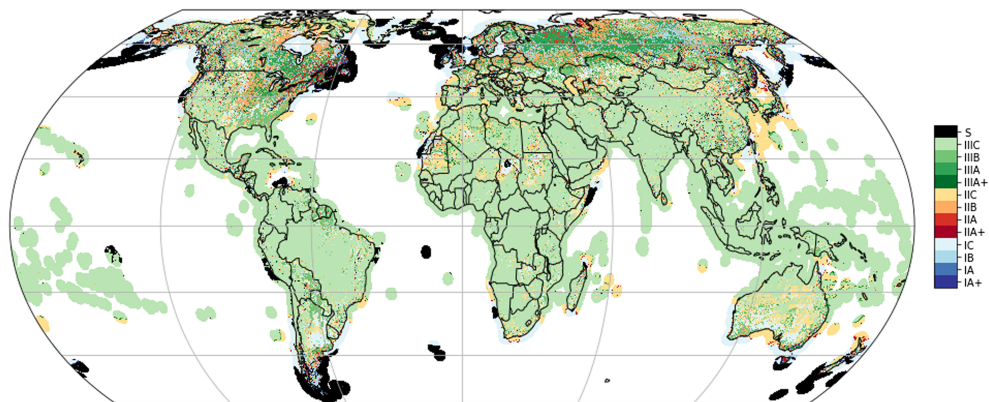


FIGURE 8 The FLS design classes at 100 m at a spatial resolution of 275 m, over all land and water (200 km from coastline)

TABLE 3 Distribution of ULS design class, global and the Denmark example

ULS class	S	Tropical	I	II	III
Global Fraction	2%	2.7%	8.3%	8.1%	78.9%
Denmark Fraction ^a	0%	6.3%	42.1%	20.8%	30.8%

^aDenmark proper + GASP covered share of its exclusive economic zone (EEZ) as defined in Flanders Marine Institute.⁴⁷

TABLE 4 Spatial distribution of FLS design classes

(a)					(b)				
FLS class	I	II	III	S	FLS class	I	II	III	S
A+	0.5%	0.4%	0.8%		A+	0.8%	0.3%	0.5%	
A	0.7%	1.4%	4.2%		A	0.7%	0.6%	0.5%	
B	2.9%	5.3%	7.0%		B	1.6%	3.2%	1.8%	
C	10.7%	10.4%	50.8%		C	41.1%	19.1%	0.9%	
				4.9%					28.9%
(c)									
FLS class	I	II	III	S					
A+	0.8%	0.5%	0.6%						
A	1.8%	14.5%	2.0%						
B	12.3%	6.5%	<0.1%						
C	31.8%	<0.1%	<0.1%						
				29.2%					

Note: (a) global, wake effects included; (b) Denmark, without wake effects; and (c) Denmark, wake effects included. The definition of Denmark is the same as in Table 3.

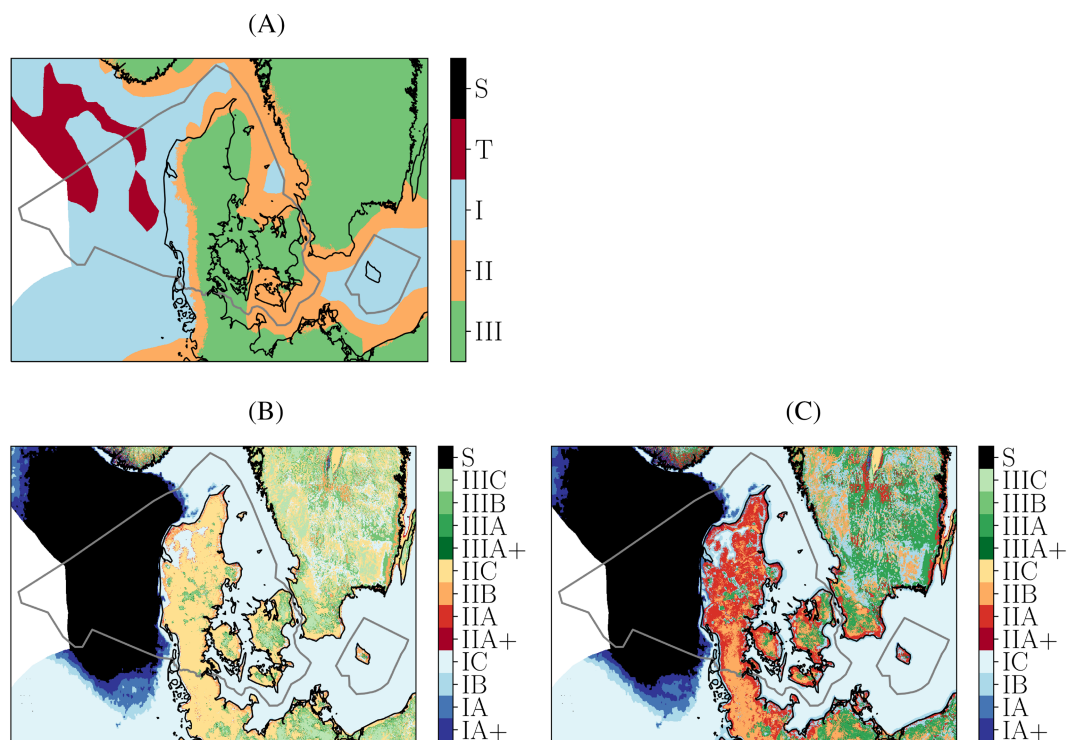


FIGURE 9 Distribution over Denmark and surrounding area of (A) the ULS design classes at 100 m; (B) the FLS design class at 100 m, without wake effects; (C) the FLS design class at 100 m, with wake effects. The gray line indicates the area (Denmark proper + EEZ) considered for the statistics in Tables 3 and Table 4

Figure 7 and Table 3 suggest that, globally, the majority of land is class III. Corresponding statistics are different in different regions and areas. We use Denmark and surrounding area as an example for a close-up analysis; see Figure 9 and corresponding statistics in Tables 3 and 4b,c. This area of limited extent has a rather complex coastline and strong gradients in the wind climate. The ULS classes are shown in Figure 9A, and FLS, with and without wake effects, is shown in Figure 9B,C, respectively. It can be seen that there is a transition from class III in eastern Denmark over

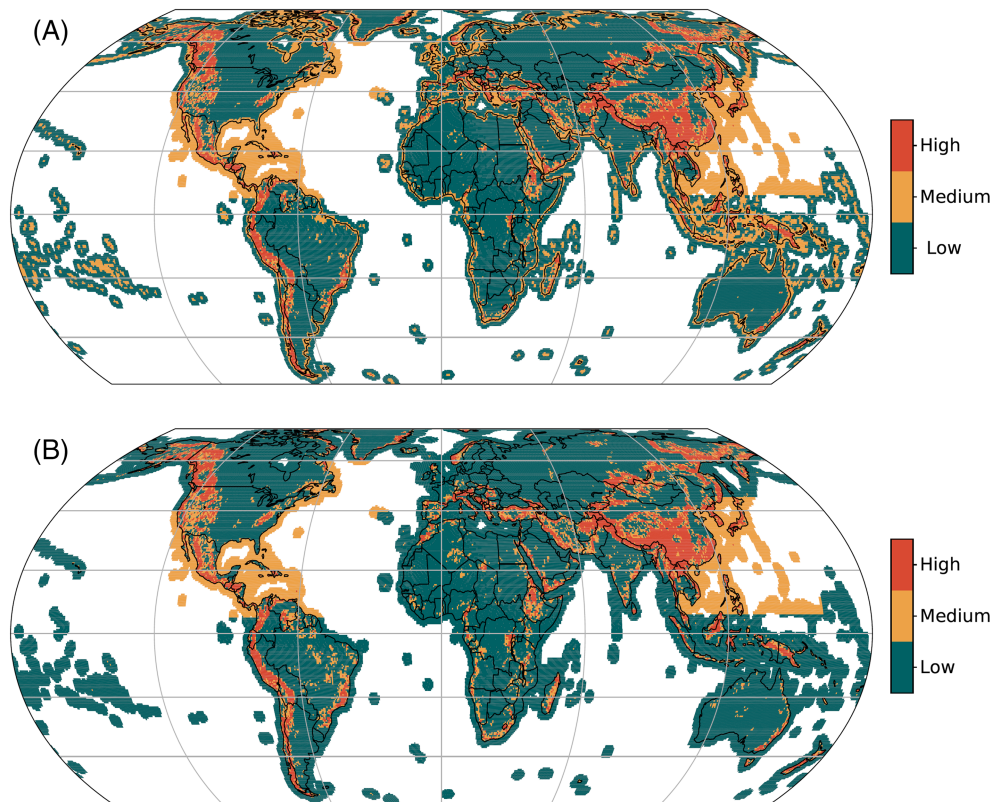


FIGURE 10 Global distribution of uncertainty class: low, medium, and high for (A) the 50-year wind at 100 m and (B) the turbulence at 100 m

a narrow band of class II to class III along the west coast and in the North Sea. Further to the open sea a region of “tropical” class appears to be required. However, most offshore projects have a scale where custom designed S-turbines are feasible.

The collection of the uncertainty class index calculated for all model grid points is divided into three categories. The three traffic light color codes are presented in Figure 10A for showing three degrees of reliability of the estimation of the 50-year wind. Similarly, the corresponding color codes are presented in Figure 10B for the turbulence. For both plots, one can see the box-shape with sharp color change over the Southern North-Pacific ocean. This is because this is one of the 16 categories as “tropical cyclone affected area,” where the lists of parameters and the corresponding methods used are different from surrounding areas (see Section 3.3.1).

5 | VALIDATION

5.1 | 50-year wind validation

The validation of the 50-year wind used published atlases from South Africa, based on measurement stations across the country and results from mesoscale modeling, using the Weather Research and Forecasting (WRF) model, with a horizontal spatial resolution of 3.3 km, as published in Larsén et al.⁴⁸ In order to compare with the published atlas of the 50-year wind at 10 m, which were based on more than 70 measurement sites (Figure 11C; from Kruger⁴⁹), we extrapolate the GASP values to 10 m from 50, 100, and 150 m through a logarithmic fit with height. The spatial distribution of the 50-year wind at 10 m from the three data sources is shown in Figure 11A–C. Both the mesoscale WRF and GASP capture the spatial distribution shown from the measurements, including the locations of the largest winds. While a systematic overestimation can be seen in the WRF data, the GASP results show better agreement with the measurements, e.g., the areas where the 50-year wind is in the ranges of 10–15 and 15–20 m s⁻¹ (cf. Figure 11A,C).

In addition to the qualitative map based evaluation, the distribution of the difference between the modeling and measurements, $\Delta U_{50} = U_{50,MOD} - U_{50,OBS}$ is shown in Figure 11D. Here, in addition to the stations from Figure 11C, newer data are used too. In total, there are 120 stations including 9 stations with measurements at 60 m and the rest are at 10 m. The mean value of ΔU_{50} of the WRF model is 3.5 m s⁻¹, confirming an overall overestimation, while the mean value of ΔU_{50} for the GASP modeling is -1.5 m s⁻¹, suggesting a slight overall

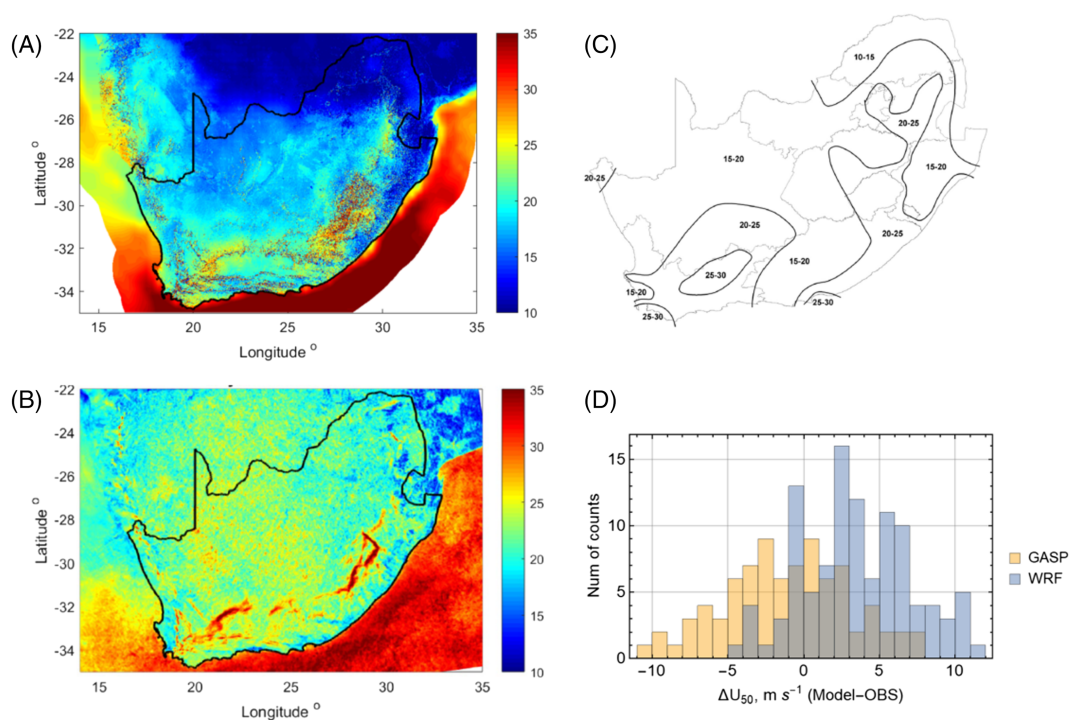


FIGURE 11 Validation of the GASP extreme wind: spatial distribution of the 10-min values of 50-year wind (A) from GASP at 10 m; (B) from WRF modeling at 10 m, from Larsén et al. (2021c)⁴⁸; (C) from measurements at 10 m, from Kruger (2010)⁴⁹; (D) Distribution of the difference in U_{50} at measurement heights (10 m and 60 m) between both WRF and GASP modeled values and measured values, at 120 stations

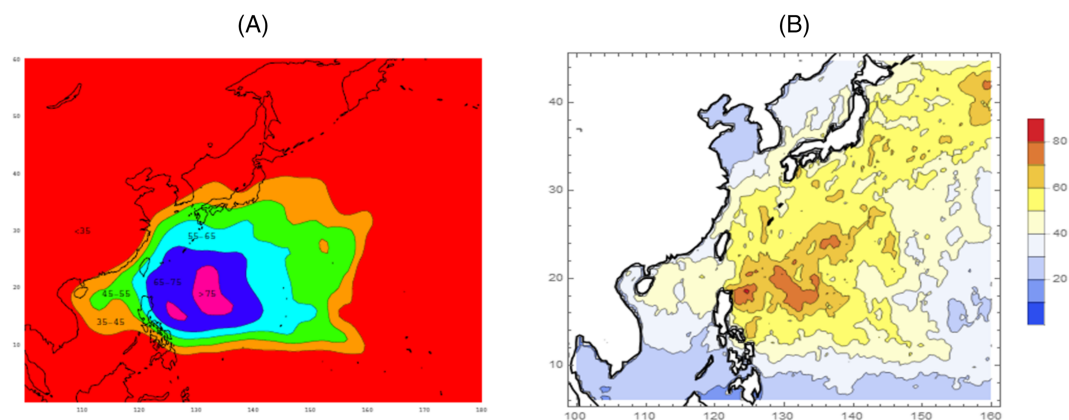


FIGURE 12 Spatial distribution of the 50-year wind at 10 m over the Southern North Pacific Ocean from (A) Ott (2005)²⁶; (B) from GASP

underestimation. As seen in the maps, the GASP results are more similar in magnitude to the measured extreme winds. Possible reasons why WRF overestimates the winds could be because that the WRF data are of a spatial resolution of 3 km, which is not able to resolve the local effects, or because the setup of WRF can favor the overestimation of storm winds. It is however beyond the scope of the current study to go deep into the WRF analysis. Finally, the correlation coefficient between the measurements and both models was calculated, with a value of 0.64 for WRF, and, only slightly higher, at 0.68 for GASP.

The calculations of the 50-year wind at 10 m were prepared over the Southern North Pacific Ocean, in order to compare with the results from Ott,²⁶ which was obtained from best track data and Holland model, and validated with the Philippine extreme wind atlas from measurements. The comparison of GASP results and Ott²⁶ is shown in Figure 12, which suggest that the GASP calculation is successful. Not only do the GASP results capture the spatial distribution of the 50-year wind, they also capture the wind strength as in Ott.²⁶ The GASP results show more spatial variability, due to higher spatial resolution of the CFSR data in comparison with data from Ott (2005), which is equivalent to 200 km.

5.2 | Turbulence validation

Turbulence parameters in GASP were validated based on their applicability for load calculations, using the method described in section 3.5. Load calculations were carried out using both measured turbulence parameters and those estimated from GASP at 16 stations, both with and without the inclusion of turbine wake effects. Four components were examined: blade root flap-wise bending; low speed shaft torque; yaw bearing tilt; tower bottom fore-aft bending, with the evaluation being based on two parameters: the fatigue load at the site divided by the fatigue load for IEC Class 2B, and the relative difference of the load based on GASP and measurements (denoted as δ_{load}). Without taking wakes into account, the mean δ_{load} at the 16 sites for the four components ranged between 0% to 7%, and the standard deviation ranged between 0% to 10%. With the wake effect taken into consideration, the mean value δ_{load} at the 16 sites for the four components ranges between 0% to 3%, and the standard deviation ranges between 0% to 5%. The positive bias for both suggests that the overall estimation is slightly conservative, which is favorable for the determination of turbine class.

6 | DISCUSSION

The GASP project compiled existing data sets and methodologies in combination with additional justifications, so that it became possible to launch a global scale calculation of important siting parameters at a spatial resolution as fine as 275 m.

Such a global scale calculation has earlier been done to obtain the resource assessment data (e.g., mean wind speed, Weibull distribution, mean power density, and more) in the Global Wind Atlas projects. While both data are relevant for e.g. financial assessment studies, the GASP data parameters will provide additional insights for, e.g., wind turbine safety assessments. It must be noted that GASP project benefited from the many layers of high resolution data prepared in the GWA projects, among others the topography, roughness length and mean wind statistics.

As pointed out in Section 1, there have been studies involving global extreme wind data sets. However, they are not directly useful for siting purposes due to their comparatively low spatial resolution on the order of tens of kilometers. The GASP project, for the first time, brings a global coverage at high resolution of the most important siting parameters, including both the extreme wind and turbulence as well as turbine class recommendations to an open portal. Such an achievement benefited not only from the publicly available and global coverage of reanalysis products, but also a symphony of models for downscaling to the local scale with grid spacing of 275 m resolution and the preparation of parameters in close agreement with the IEC standard. These models include the microscale model LINCOM for the flow at local scale, the statistical model for the spectral correction method, models for turbulence and models for different loads (see Section 3). Here the use of the spectral correction method has also been adjusted to strong convection conditions and tropical cyclone affected areas that have most best track data. In addition, we developed an uncertainty classification model to address the potential issues related to such a complex modeling system, which honestly maps areas of difficulties within the frame of current methodologies.

As the whole calculation system is rather complex and complicated, assumptions have been made, which have been taken into consideration in the uncertainty assessment. These assumptions include negligible spatial variability over water within the reanalysis spatial resolution of about 40 km and neutral stability conditions. Since we downscale from reanalysis directly to local scale (cf. model chain in Figure 2), it is expected that some mesoscale features finer than 40 km are likely absent in the final results. However, in the uncertainty assessment, we did not include uncertainties related to climate type and prevalence of thunderstorms, leading to uncertainty in places such as Madagascar and Southwest Indian Islands is low, which might be overconfident. Therefore, the GASP atlas can be used as a vital departure point in the determination of wind turbine class, but preferably be backed up in the future by tropical cyclone statistics (where these are prevalent) and observational data where possible.

The validation performed here are only on the 50-year wind and turbulence related parameters over limited areas and stations. They are overall rather promising, but this shall merely be seen as a start, and more validation and feedback is needed from users.

7 | CONCLUSIONS

For the first time, a global scale, complex calculation of wind turbine siting parameters is performed via downscaling the flow from a spatial resolution of 40 km to a local scale of 275 m. The calculation provides a suit of parameters, including flow inclination, shear exponent, air density for extreme winds, the 50-year wind at three heights (50, 100, and 150 m), turbulence and wind turbine class recommendations at a spatial resolution of 275 m. The wind turbine class recommendations are based on multiple relevant reference turbines, and account for main load bearing components such as the blades and tower.

The data are shared on an open data portal.⁴⁶ These data and atlases will benefit authorities and the industries broadly as a first-line estimate of turbine design class to make fast, initiative decision when prospecting sites in new regions.

ACKNOWLEDGEMENTS

This study is supported by the Danish EUDP J. nr. 64018-0095. We thank our colleagues Morten Nielsen and Jake Badger from DTU and Morten Thøgersen from EMD for discussions.

PEER REVIEW

The peer review history for this article is available at <https://publons.com/publon/10.1002/we.2771>.

DATA AVAILABILITY STATEMENT

The global atlases data are openly available at https://data.dtu.dk/articles/dataset/Global_Atlas_of_Siting_Parameters_V1/14753349, with doi:10.11583/DTU.14753349.

ORCID

Xiaoli Guo Larsén  <https://orcid.org/0000-0001-8696-0720>

Ásta Hannesdóttir  <https://orcid.org/0000-0003-3399-4526>

Mark Kelly  <https://orcid.org/0000-0003-2882-4450>

REFERENCES

1. Fingersh L, Hand M, Laxson A. Wind turbine design cost and scaling model. *Technical report*. NREL/TP-500-40566, National Renewable Energy Lab; 2006.
2. IEC. IEC 61400-1 Ed4: Wind turbines—part 1: design requirements. *standard*. Geneva, Switzerland, International Electrotechnical Commission; 2019.
3. Eurocode. basis of design and actions on structure—parts 2–4: actions on structure—wind actions, Rue de Stassart, Brussels, European Committee For Standardization Technical Report; 1995.
4. Miller C. A once in 50-year wind speed map for Europe derived from mean sea level pressure measurements. *J Wind Eng Ind Aerodyn*. 2003;91:1813-1826.
5. Frank HP. Extreme winds over Denmark from the NCEP/NCAR reanalysis. Risø-R-1238(EN), Roskilde, Denmark, Risø National Laboratory; 2001. <http://www.risoe.dk/rispubl/VEA/ris-r-1238.htm>
6. Larsén XG, Mann J. Extreme winds from the NCEP/NCAR reanalysis data. *Wind Energy*. 2009;12(6):556-573. doi:10.1002/we.318
7. Pryor SC, Bartelmie RJ. A global assessment of extreme wind speeds for wind energy applications. *Nat Energy*. 2021;6:268. doi:10.1038/s41560-020-00773-7
8. Skamarock WC. Evaluating mesoscale NWP models using kinetic energy spectra. *Mon Weather Rev*. 2004;132:3019-3032.
9. Larsén XG, Ott S, Badger J, Hahmann AH, Mann J. Recipes for correcting the impact of effective mesoscale resolution on the estimation of extreme winds. *J Appl Meteorol Climatol*. 2012;51(3):521-533. doi:10.1175/JAMC-D-11-090.1
10. Bastine D, Larsén XG, Witha B, Dörenkämper M, Gottschall J. Extreme winds in the new european wind atlas. *J Phys Conf Seris*. 2018;1102(012006).
11. Floors R, Nielsen M. Estimating air density using observations and re-analysis outputs for wind energy purposes. *Energies*. 2019;12(11):2038. doi:10.3390/en12112038
12. Astrup P, Larsen SE. WAsP Engineering flow model for wind wind over land and sea. Risø-R-1107, Roskilde, Denmark, www.risoe.dk, RisøNational Laboratory; 1999. www.risoe.dk.
13. Astrup P, Jensen NO, Mikkelsen T. Surface roughness model for lincom. 900(EN), Denmark, Forskningscenter Risø. Risø-R; 1996.
14. Saha S, Moorthi S, Pan H-L, et al. The ncep climate forecast system reanalysis. *Bull Am Meteorol Soc*. 2010;91(8):1015-1058. doi:10.1175/2010BAMS3001.1
15. Rienecker MM, Suarez MJ, Gelaro R, et al. Merra: NASA's modern-era retrospective analysis for research and applications. *J Clim*. 2011;24(14):3624-3648. doi:10.1175/JCLI-D-11-00015.1
16. Hersbach H, Bell B, Berrisford P, et al. The era5 global reanalysis. *Quarterly Journal of the Royal Meteorological Society*. 2020;146(730):1999-2049. doi:10.1002/qj.3803
17. Hansen BO, Larsén XG, Kelly M, et al. Extreme wind calculation applying spectral correction method—test and validation. DTU Wind Energy E-0098, Wind Energy Department, Technical University of Denmark; 2016.
18. Larsén XG, Kruger A. Application of the spectral correction method to reanalysis data in South Africa. *J Wind Eng Ind Aerodyn*. 2014;133:110-122.
19. Larsén XG, Davis N, Hannesdóttir A, et al. Calculation of global atlas of siting parameters. DTU Wind Energy E-0208, Denmark, DTU Wind Energy Department; 2021.
20. Wessel P, Smith WHF. A global, self-consistent, hierarchical, high-resolution shoreline database. *J Geophys Res*. 1996;101(B4):8741-8743.
21. Troen I, Petersen EL. European wind atlas, Denmark, Risø National Laboratory, Roskilde; 1989. http://orbit.dtu.dk/files/112135732/European_Wind_Atlas.pdf
22. Badger J, Frank H, Hahmann AN, Giebel G. Wind-climate estimation based on mesoscale and microscale modeling: Statistical-dynamical downscaling for wind energy applications. *J Appl Meteorol Climatol*. 2014;53(8):1901-1919. doi:10.1175/JAMC-D-13-0147.1
23. Landberg L, Myllerup L, Rathmann O, Petersen EL, Jørgensen BH, Badger J, Mortensen NG. Wind resource estimation - An overview. *Wind Energy*. 2003;6:261-271.
24. Mann J, Ott S, Jørgensen B, Frank H. WAsP Engineering 2.0. Risø-R-1356(EN), Roskilde, Denmark, Risø National Laboratory; 2002. <http://www.risoe.dk/rispubl/VEA/ris-r-1356.htm>
25. Larsén XG, Vincent CL, Larsen S. Spectral structure of the mesoscale winds over the water. *Q J R Meteorol Soc*. 2013;139:685-700. doi:10.1002/qj.2003

26. Ott S. Extreme winds in the western North Pacific. Risoe-R-1544(EN), Roskilde, Denmark, Risø National Laboratory; 2005. www.risoe.dk/rispubl/VEA/veapdf/ris-r-1544.pdf.
27. Larsén XG, Ott S. Adjusted spectral correction method for calculating extreme winds in tropical cyclone affected water areas. *Wind Energy Sci.* 2022. in review
28. Charnock H. Wind stress on a water surface. *Q J R Meteorol Soc.* 1955;81:639-640.
29. Andreas EL, Mahrt L, Vickers D. An improved bulk air-sea surface flux algorithm, including spray-mediated transfer. *Q J R Meteorol Soc.* 2015;141:642-654. doi:10.1002/qj.2424
30. Zijlema M, van der Westhuysen AJ. On convergence behaviour and numerical accuracy in stationary SWAN simulations of nearshore wind wave spectra. *Coast Eng.* 2005;52(3):237-256. doi:10.1016/j.coastaleng.2004.12.006
31. Hill C, DeLuca C, Balaji, Suarez M, Da Silva A. The architecture of the Earth system modeling framework. *Comput Sci Eng.* 2004;6(1):18-28. doi:10.1109/MCISE.2004.1255817
32. Kaimal JC, Wyngaard JC, Izumi Y, Coté OR. Spectral characteristics of surface-layer turbulence. *Q J R Meteorol Soc.* 1972;98:563-589.
33. Floors R, Enevoldsen P, Davis N, Arnqvist J, Dellwik E. From lidar scans to roughness maps for wind resource modelling in forested areas. *Wind Energy Sci.* 2018;3(1):353-370. doi:10.5194/wes-3-353-2018
34. Kelly M, Larsen G, Dimitrov NK, Natarajan A. Probabilistic meteorological characterization for turbine loads. *J Phys Conf Ser.* 2014;524(1):012076. doi:10.1088/1742-6596/524/1/012076
35. Nieuwstadt FTM. The turbulent structure of the stable, nocturnal boundary layer. *J Atmos Sci.* 1984;41(14):2202-2216.
36. Kelly M, Wyngaard JC, Sullivan PP. Application of a subfilter-scale flux model over the ocean using OHATS field data. *Journal of the Atmospheric Sciences.* 2009;66(10):3217-3225.
37. Kelly M, Troen I. Probabilistic stability and "tall" wind profiles: theory and method for use in wind resource assessment. *Wind Energy.* 2016;19(2):227-241.
38. Kelly M. Estimation of local turbulence intensity via mesoscale stability and winds, with microscale shear and terrain. E-0213(EN), Roskilde, Denmark, Wind Energy Dept., Risø Lab/Campus, Danish Tech. Univ. (DTU); 2020.
39. Kelly M, Kersting G, Mazoyer P, Yang C, Fillols FH, Clark S, Matos JC. Uncertainty in vertical extrapolation of measured wind speed via shear. E-0195 (EN), Roskilde, Denmark, Wind Energy Dept., Risø Lab/Campus, Danish Tech. Univ. (DTU); 2019.
40. Toft HS, Svenningsen L, Moser W, Sørensen JD, Thøgersen ML. Assessment of wind turbine structural integrity using response surface methodology. *Eng Struct.* 2016;106:471-483.
41. Malcolm DJ, Hansen AC. Windpact turbine rotor design study. NREL/SR-500-32495, Golden, CO, National Renewable Energy Laboratory; 2006.
42. Jonkman JM, Butterfield S, Musial W, Scott G. Definition of a 5-mw reference wind turbine for offshore system development. NREL/TP-500-38060, Golden, CO, National Renewable Energy Laboratory; 2009.
43. Bak C. Description of the dtu 10 mw reference wind turbine. DTU Wind Energy Report-I-009, Roskilde, Denmark, DTU Wind Energy; 2013.
44. Jonkman JM. Fast an aeroelastic computer-aided engineering (cae) tool for horizontal axis wind turbines, Golden, CO, National Renewable Energy Laboratory; 2013. <https://nwtc.nrel.gov/FAST>
45. Larsén XG, Imberger M, Davis N, Kelly M, Hannesdóttir A. Uncertainty classification of the global atlases for siting parameters. 0221, Denmark, DTU Wind Energy; 2021.
46. Larsén XG, Davis N, Hannesdóttir A, et al. Global atlas of siting parameters v1, dataset, Denmark, DTU Wind Energy Department; 2021. doi:10.11583/DTU.14753349
47. Flanders Marine Institute. Union of the esri country shapefile and the exclusive economic zones (version 3). Available online at <http://www.marineregions.org/>; 2020.
48. Larsén XG, Kruger A, Floors R, Cavar D, Hahmann A. Atlas of extreme wind and gust for south africa. DTU Wind Energy E-0220, Roskilde, Denmark, DTU Wind Energy Department; 2021.
49. Kruger A. Wind climatology of South Africa relevant to the design of the built environment. *PhD dissertation*: Stellenbosch University; 2010. <http://hdl.handle.net/10019.1/6847>

How to cite this article: Larsén XG, Davis N, Hannesdóttir Á, et al. The Global Atlas for Siting Parameters project: Extreme wind, turbulence, and turbine classes. *Wind Energy.* 2022;25(11):1841-1859. doi:10.1002/we.2771